High-Expansion-Ratio Deployable Space Structures for Long Duration Space Missions

Mitchell B. Fogelson*
Mechanical Engineering
Carnegie Mellon University
Pittsburgh, USA
mfogelson@cmu.edu

Sawyer Thomas*
Mechanical Engineering
University of Washington
Seattle, USA
sawyermt@uw.edu

Giusy Falcone
Robotics Institute
Carnegie Mellon University
Pittsburgh, USA
gfalcone@andrew.cmu.edu

Jeffrey I. Lipton
Mechanical Engineering
Northeastern University
Boston, USA
j.lipton@northeastern.edu

Zachary Manchester
Robotics Institute
Carnegie Mellon University
Pittsburgh, USA
zacm@cmu.edu

***Abstract*— Artificial gravity is a crucial technology to enable long-duration human space flight. However, a kilometer-scale rotating space structure is needed to generate artificial gravity at rotation rates that can be tolerated comfortably by crew. Constructing such a structure with current technology would require many launches and significant in-space assembly. This work presents HERDS, High-Expansion-Ratio Deployable Structures, a hierarchical expansion mechanism that can deploy a kilometer-scale structure from a single launch. HERDS leverages a hierarchical combination of a Kresling mechanism and a pop-up extending truss (PET), a novel variant of the scissor mechanism. We show that HERDS designs achieve 4-11x better beam member aspect ratios than non-hierarchical Kresling or scissor mechanisms, resulting in a stiffer deployed structure. Furthermore, HERDS designs are shown in simulation to satisfy the necessary loading and structural constraints for supporting the Lunar Gateway mission with a factor of safety greater than 1.5 using existing launch vehicles. Our modeling and analysis is validated on a 1/10 scale prototype with a 50x expansion ratio.**

TABLE OF CONTENTS

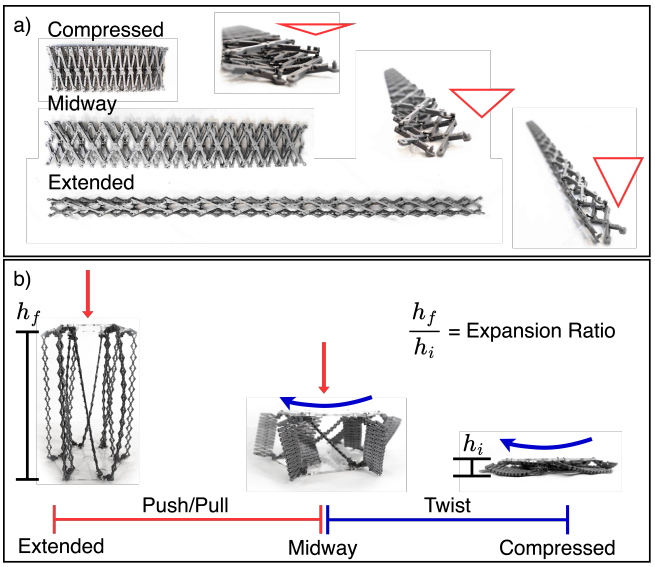

Figure 1. a) Three phases of the pop-up extending truss (PET) mechanism. In its compact form, the cross section is nearly flat. As it expands, its cross section becomes a triangular shape, as shown in red, improving its inertia and stiffness. b) HERDS utilizes a nested design in which PET mechanisms form the beams of a Kresling structure. The spiral collapse of the Kresling design allows the PETs to pack neatly in their compact, flat configuration. Combining both mechanisms makes it possible to achieve very high expansion ratios, enabling the deployment of massive kilometer-sized structures from a single launch vehicle.

1. INTRODUCTION

Long-duration spaceflight poses serious challenges for the human body, including muscle atrophy, bone loss [1, 2], eyesight degradation [3], and immunosuppression [4, 5]. Many of these effects are linked to a lack of gravity, and the ability to generate artificial gravity with a rotating space structure would eliminate their root cause [6]. Concepts for rotating space habitats to generate artificial gravity date back over a century [7]. Such a structure must be able to rotate at rates around 1-2 RPM as humans experience discomfort from exposure to rotation rates as low as 3 RPM [8, 9]. To achieve a centripetal acceleration equivalent to Earth's gravity (i.e., $a = 9.81 m/s^2$) at 1 RPM, a 1.7-kilometer-long structure is required. A half-kilometer-long structure is needed for a spinning rate of 2 RPM, which is generally considered an upper bound for human comfort. This study, therefore, aims to evaluate the feasibility of kilometer-scale rotating structures.

A kilometer-scale space structure using current technologies would require dozens of launches of SpaceX's Falcon Heavy given the fairing capacity [10]. In addition, significant on-orbit assembly and fabrication would drastically increase risk

*Both authors contributed equally to this work.

This work was supported by a NIAC award from NASA's Space Technology Mission Directorate (Grant Number 80NSSC21K0446)

and cost. In principle, a long tether can be used to deploy a rotating space habitat from a single launch [11]. However, tethers have limited ability to transmit mechanical loads, making maneuvering and station-keeping control difficult.

This work presents a novel hierarchical mechanism, shown in Figure 1, that combines two one-degree-of-freedom mechanisms, specifically a Kresling mechanism with pop-up expanding trusses (PET), a novel scissor mechanism variant. This system achieves the expansion ratios capable of deploying a kilometer-scale structure with no in-space assembly, supporting mechanical loads when fully extended, and leveraging redundancy in both substructures to mitigate deployment failures. This paper makes the following contributions:

1. A hierarchical approach for achieving large expansion ratios with enhanced mechanical stiffness properties (HERDS).
2. A novel mechanism that enables efficient packing of pop-up extending truss systems (PET).
3. A mixed-integer nonlinear optimization formulation to enable design optimization for various mission constraints.
4. Simulation and hardware validation of the HERDS system.

The paper is organized as follows: Section 2 reviews other deployable structures that either have been investigated for this application or provide useful points of comparison. Section 3 begins with examining the Lunar Gateway project and extracting the mission-specific constraints for a deployable structure. This includes thrust requirements for maneuvers, payload requirements for habitat areas, and factor of saftey requirements. Next, Section 4 discusses the novel HERDS design and proposes an optimization formulation for enabling design variants for various contexts. Section 5 shows how the substructures and superstructures meet the necessary structural requirements through analysis and simulation. Section 6 describes hardware prototypes that were constructed and tested to validate our modeling and analysis. Finally, we summarize our conclusions and directions for future work in Section 7.

2. Related Work

Deployable Structures

Booms—Booms are a critical part of space infrastructure. As detailed in [12, 13] numerous boom technologies exist but are still limited by their unpredictable deployability. Their reliance on tensioning cables or buckling elements to deploy and maintain shape is also a key limitation of these technologies.

Tensegrity—Tensegrity designs pack well and are conceptually simple. However, they have two major flaws: first, they rely on cables that only become taut when fully deployed, making tangling during deployment possible [14, 15]. Second, they lack redundancy, and the failure of a single cable can significantly weaken the structure [14, 15].

Tethers—Tethers are perhaps one of the most straightforward space structures and have been tested in orbit numerous times. Most notably, the Gemini 11 mission deployed a 100-foot (30-meter) tether between the crewed Gemini capsule and the Agena upper-stage booster. This then spun the combined system up to a rotation rate of 55 degrees per minute to produce an artificial gravity of approximately 0.00015g [16]. Other notable on-orbit tether deployments include the two Space Shuttle TSS missions flown in 1992 and 1996 [17] that attempted to deploy a 20 km electrodynamic tether. All three of these experiments encountered difficulties dealing with tethers' inherently flexible nature and inability to transmit mechanical loads. In the case of Gemini 11, substantial oscillations were produced in the tether during the deployment and spin-up process. In the case of the two shuttle experiments, the tether became stuck during deployment in one case and was severed in the other shortly before reaching full deployment. These difficulties motivate our investigation of rigid structures.

Table 1. Payload Fairing Dimensions and Mass Limits for Falcon, Starship, Starship Extended, SLS B1, and SLS B2 Space Vehicles

	Falcon [10]	Starship [22]	Starship Ext. [22]	SLS B1 [23]	SLS B2 [23]
Height	9.7 m	17.2 m	22 m	19.0 m	27.8 m
Diameter	3.4 m	4.4 m	4.4 m	8.4 m	8.4 m
Mass	10 t	21 t	21 t	42 t	46 t
Exp. Ratio	103.6	58.8	45.45	52.6	35.9

Buckling— Buckling-based designs come in many forms: Those based on a wrapping design, like the Storable Tubular Extendible Members (STEM) or Spiral Tube and Actuator for Controlled Extension/Retraction (STACER), can have very high packing density but have low strength [18]. Coilable masts, used in the NuStar and Shuttle Radar Topography Mission, are limited by their inherent need for structures to be easily buckle-able for storage [19]. The major issue with these designs for a kilometer-scale structure is the sheer amount of stored energy in the system while packed for launch: Four straight two-inch diameter beams 1 km long in a buckled state would store 34.6 million Joules of energy, or the equivalent of 7.4 kg of TNT. A single error in containment would be catastrophic. While less than ideal for larger size scales and loads, the success of the NuStar and Shuttle Radar topography missions show that making a complex, space-worthy structure with a large number of joints is possible [20]. To make a kilometer-scale structure, however, a design is needed that will not be limited by its deployment method reliability or energy storage.

3. Mission Context

Background

The NASA Lunar Gateway program is an ambitious initiative to establish a sustainable, modular space station in orbit around the Moon [21]. That outpost will serve as a staging point for long-term crewed explorations of the lunar surface and, potentially, as a stepping-stone for missions to farther destinations such as Mars. HALO, a central component of NASA's Gateway program, will serve as living quarters for astronauts and a hub for command, control, power distribution, and scientific research, including communication with lunar surface missions [21]. In this work, Lunar Gateway is used as a case study to demonstrait that the HERDS design can satisfy system constraints and be a potential solution in future missions to support astronauts' physiological health during extended missions.

Space Vehicle Constraints

While launch costs are steadily falling, enabling a single-launch deployable structure avoids the risk, complexity, and

cost of in-space assembly. We considder five launch configurations: the SpaceX Falcon Heavy [10], SpaceX Starship [22], SpaceX Starship Extension [22], Boeing's Space Launch System Block 1 (SLS B1), and Space Launch System Block 2 (SLS B2) [23]. We calculate the requisite expansion ratios using existing payload fairing dimensions provided by the respective vehicle manufacturers, detailed in Table 1. Based on this data, the initial diameter of the structure ranges from 3.4m-8.4m, the initial height ranges from 9.7m-27.8m, and the maximum mass of the structure ranges from 10–46 tonnes. Therefore, expansion ratios of 36–100x are necessary to reach the final 1 km length goal, with constraints set by launch vehicles' fairing dimensions.

Structural Considerations

For a structure to support the Lunar Gateway missions, we consider the thrust, payload, and factor of safety (FoS) requirements shown in Table 2. Thrusters capable of exerting up to 300 N forces are assumed in both compressive and tangential directions, stemming from components used on the ISS [24]. Additionally, the structure must support habitat modules like I-HAB and HALO. These systems are estimated to be 10t per current habitat specifications or 20t if two habitats are attached [25]. Adhering to the recommended safety factors for aerospace structures, this system should support a FoS range from 1.4 to 1.5 as outlined in [26].

Table 2. **Expected Thrust, Payload, and Factor of Safety (FoS) Specifications for a Lunar Gateway Mission Support Structures**

Thrust Loads	Payload [25]	FoS [26]
300 N	10-20 t	1.4-1.5

4. HERDS DESIGN

Designing a structure that can extend to a kilometer in length requires extremely efficient use of available space, with high material packing density in the stowed state. For a deployable structure with a set width, high expansion ratios can typically be achieved only by reducing the thickness of the constituent members. As a result, configurations meeting the desired extension requirements often exhibit high beam length-to-width aspect ratios, making them prone to local buckling. In this section, we describe the combination of the pop-up extending truss — a novel scissor mechanism variant shown in Figure 2 — and the Kresling mechanism, to make high expansion ratio deployable structures (HERDS).

Pop-up Extending Truss

The scissor mechanism, a straightforward one-degree-of-freedom system, exhibits favorable expansion capabilities. One limitation of a conventional scissor mechanism is that, as the system extends, the cross-sectional area decreases, leading to a low bending moment of inertia and poor stiffness. To enhance rigidity, several variants exist, including a branched scissor mechanism with three-way symmetry [27], a branched scissor mechanism with four-way symmetry [27], as well as connecting three scissor mechanisms in a triangular configuration, seen in Figure 3. For these systems to achieve high expansion ratios, they must have undesirable high length-to-width ratios. Given the symmetry of these designs, reorienting the systems doesn't offer any advantage in minimizing the overall packing.

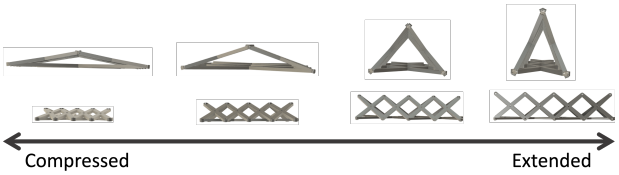

Figure 2. The Pop-up extending truss through various phases of expansion. The top set of images shows how the cross-section changes as the scissor system expands

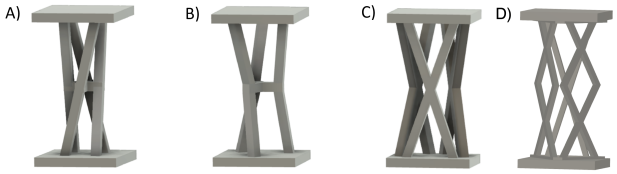

Figure 3. A) Branched Scissor Mechanism 4 way symmetry [27] B) Branched Scissor Mechanism 3 way symmetry [27] C) Tri-Scissor Mechanism D) Pop-up Expanding Truss (PET)

To address these issues, we developed the pop-up extending truss (PET). Its compressed state lies flat and "pops up" as it transitions to the expanded state, forming a triangular cross-section, seen in Figure 2. The PET is a one-degree-of-freedom deployable structure that extends like a typical scissor mechanism, but the triangular cross-sectional area in its deployed state provides favorable inertial and stiffness properties. We note that other cross-sectional geometries, such as quadrilateral or polygon-variant, can be achieved by mirroring the members or other manipulations to the triangular variant. This paper and design focuses on the simplest system description the triangular PET.

Cell Load Test—A PET cell has comparable performance to other scissor variants, with the added benefit of flattening in the stowed state. A finite-element analysis (FEA) comparison of an expanded PET cell to a tri-scissor cell and branching scissor cells with three- and four-way symmetry is evaluated. All cells are considered rigid structures with the same height, member thickness, and material. Cell-specific parameters were chosen to make each unit cell as similar as possible. Using Ansys®Academic Research Mechanical, Release 22.2 [28] static structural analysis tools, a fixed support is applied to the bottom face of the cell, and a fixed displacement is applied to the top face. A negative displacement measures the compressive stiffness of the cell, and in a different test, a horizontal displacement measures the bending stiffness. The results from these experiments can be seen in Table 3. These results show that the PET cell is stiffer than the branching scissor cells in compression and bending. However, the tri-scissor cell performs the best. This is an expected result, as the tri-scissor is a more uniform truss structure.

Table 3. **Scissor Cells Analysis in Compression and Bending**

	PET	Tri-Scissor	BSM 3	BSM 4
Compressive [N/m]	8.807e7	**1.9955e8**	2.0442e7	1.5801e7
Bending [N/m]	5.2219e5	**2.9219e6**	2.7821e5	3.1128e5

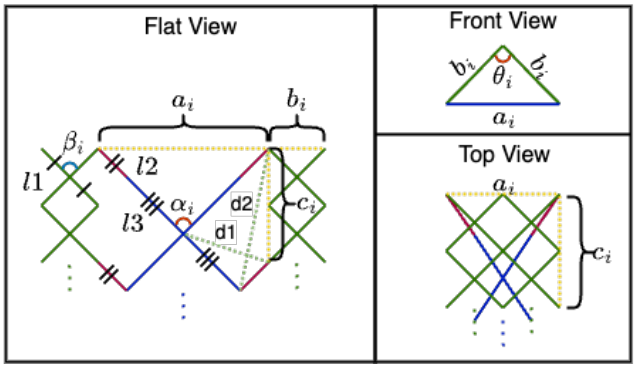

Figure 4. Wire frame diagram of a Pop-up Extending Truss

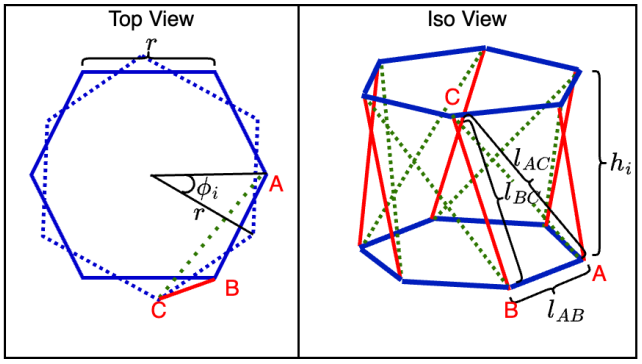

Figure 5. Wire frame diagram of Kresling mechanism, as adapted from [29]

Cell Kinematics—The PET combines two different standard scissor mechanisms connected by revolute joints. The long asymmetric scissor in the middle and the shorter scissor sides are shown in the flat view of Figure 4. The long asymmetric scissors connect with the shorter sides by two-degree-of-freedom joints. This ensures that the structure opens in a straight line. The long asymmetric scissor is described by $l2$, the offset length, and $l3$, half the scissor length. The side scissors are described by $l1$, which is half the length of the scissor. Given $l1$, $l2$, and $l3$ the PET can be fully defined with an angle α, thus making it a one-DOF mechanism. PET kinematics has a closed mathematical formulation that must be satisfied to build and design such a system without compliance.

The PET parameters are evaluated at several instances, $i = 1 : I$, of the phase angle, α_i. Given $l1$, $l2$, $l3$ and α_i the other parameters, shown in Figure 4, can all be determined through the following equation which step from the law of cosines:

$$a_i = (l2 + l3) * \sqrt{(2 * (1 - \cos(\alpha_i)))} \tag{1}$$

$$c_i = \sqrt{\begin{array}{l}(l2(\sin(\alpha_i/2) + \sin(3\alpha_i/2)))^2 \\ +(2\cos(\alpha_i/2)(l2\cos(\alpha_i) + l3))^2\end{array}} \tag{2}$$

$$\beta_i = \cos^{-1}(1 - 0.5(\frac{c_i}{2l1})^2) + \pi \tag{3}$$

$$b_i = l1 * \sqrt{(2 * (1 - \cos(\beta_i)))} \tag{4}$$

$$d1_i = \sqrt{(l3^2 + l2^2 - 2 * (l3 * l2) * \cos(\alpha_i))} \tag{5}$$

$$d2_i = \sqrt{\begin{array}{l}((l2 + l3)^2 + l3^2) \\ -2(l3(l2 + l3))\cos(\pi - \alpha_i)\end{array}} \tag{6}$$

$$\theta_i = \cos^{-1}((a_i^2 - 2 * b_i^2)/(-2 * b_i^2)) \tag{7}$$

From these parameters, the following constraints must be satisfied for the PET to be kinematically feasible:

$$a_i \leq 2 * b_i \tag{8}$$

$$c_i \leq l2 + d1_i \tag{9}$$

$$d1_i \leq l2 + c_i \tag{10}$$

$$d1_i^2 + d2_i^2 - c_i^2 - l3^2 - 2 * (l2 * (l2 + l3)) = 0 \tag{11}$$

Equations (8), (9), (10) describe triangle inequality constraints. Equation (11) describes the constraints on the trapezoid created by combining multiple PET cells seen in Figure 4. To ensure it is feasible to build such a system with members that have thickness and not simply from the idealized line model, constraints are applied to link lengths and phase angles based on member thickness t:

$$l1, l2, l3 > 0 \tag{12}$$

$$\alpha_i \leq 2\cos^{-1}(\frac{l3}{\sqrt{l3^2 + t^2}}) \tag{13}$$

$$\alpha_i \geq \pi - 2\cos^{-1}(\frac{l3}{\sqrt{l3^2 + t^2}}) \tag{14}$$

$$\beta_i \leq 2\cos^{-1}(\frac{l1}{\sqrt{l1^2 + t^2}}) \tag{15}$$

$$\beta_i \geq \pi - 2\cos^{-1}(\frac{l1}{\sqrt{l1^2 + t^2}}) \tag{16}$$

Finally, to achieve the pop-up capabilities when designing the PET, where the system fully closes and fully opens, two additional constraints can be added as follows:

$$\theta_1 = \pi \tag{17}$$

$$\theta_I = \frac{\pi}{3} \tag{18}$$

where θ_1 is the folded angle of the system, and θ_I is the final angle of the triangle in radians. The pop-up extending truss, in isolation, fails to attain a 50x expansion ratio without resorting to members with poor aspect ratios, which are prone to buckling.

Kresling Mechanism

The Kresling pattern is a popular collapsible design in origami. Zhai et al. [29] designed a mechanical metamaterial version of this system with rigid components and standard joints. Their system is comprised of two primary components: outer rigid members and inner extendable ones. They parameterized this system with the height h, the radius r, and the twist angle ϕ seen in Figure 5. The following additional parameters can be determined from the following equations:

$$l_{AB} = 2r\sin(\frac{\pi}{6}) \tag{19}$$

$$l_{BC} = \sqrt{h^2 - 2r^2\cos(\phi) + 2r^2} \tag{20}$$

$$l_{AC} = \sqrt{h^2 - 2r^2\cos(\frac{2\pi}{6} + \phi) + 2r^2} \tag{21}$$

where l_{AB} is the side length of the hexagon, l_{BC} is the length of the outer member, and l_{AC} is the extendable inner member. Zhai et al. [29] showed that this design had the favorable properties of easy collapsability through one-way rotation

Table 4. Objective value of HERDS, PET, and Kresling from MINLP optimization for all space vehicles

	HERDS	PET	Kresling
Falcon	**41.4**	312.0	481.0
Starship	**28.6**	176.0	271.0
Starship Ext.	**28.6**	138.0	212.0
SLS B1	**20.3**	159.0	246.0
SLS B2	**19.4**	109.0	168.0

and high compression stiffness when deployed. However, similar to the challenges faced by the PET, to reach high expansion ratios, the Kresling mechanism is bound by the member thickness, making it hard to attain desired expansion metrics without compromising structural integrity.

HERDS Superstructure

A hierarchical superstructure that combines the PET and Kresling mechanisms can reach high expansion ratios while maintaining desired structural properties. The HERDS hierarchical superstructure is the first the authors have seen in the literature. HERDS can consist of different combinations of mechanisms, but this section discusses the specific combination of Kresling mechanisms with PETs. The patternable cells of both the Kresling mechanism and PETs allow for the superstructure to be conceptualized as a single cell and patterned to satisfy mission constraints.

The HERDS superstructure has design constraints in addition to the kinematic constraints defined in Section 4 and Section 4. The following equations consider mission-specific constraints such as fairing size and mass requirements from Section 3:

$$D = 2l_{AB} + 2a_1 \tag{22}$$
$$a_1 < l_{AB} \tag{23}$$
$$n * c_1 = l_{BC1} = D/2 \tag{24}$$
$$n * c_f = l_{BCf} = l_{ACf} \tag{25}$$
$$m * h_1 \leq H_0 \tag{26}$$
$$m * h_f \geq H_f \tag{27}$$
$$V = 12m(2t)^2 * (8n(2l1) + 2n(2l3 + l2)) \tag{28}$$
$$\rho * V \leq M \tag{29}$$
$$n, m \in \mathbb{I} \tag{30}$$

where D the fairing diameter, H_0 the fairing height, H_f the final deployed length, M is the max payload, t is half the thickness of a member, V is an approximation for the total volume and ρ is the density of the material, n is the discrete number of PET cells, and m is discrete number of Kresling cells.

Design Optimization—The superstructure design problem has both continuous parameters and integer parameters. This problem can be formulated as the following mixed-integer nonlinear program:

$$\underset{x,\,y}{\text{minimize}} \quad \ell(x, y) \tag{31a}$$
$$\text{subject to} \quad (8) - (30) \tag{31b}$$

where $x = [l1, l2, l3, t, \alpha_{i=1:I}, r, \phi_{i=1:I}, h_{i=1:I}]$ and $y = [n, m]$ and $\ell(\cdot)$ is an objective function. The objective function can be task-specific; we chose a continuous and differentiable objective function that enables existing solvers to find solutions efficiently. The objective function,

$$\ell(\cdot) = (l1 + l2 + l3)/t, \tag{32}$$

seeks to minimize the aspect ratio of the members as long skinny members are prone to buckling. Given the design constraints of the space vehicles from Table 1 and the mission constraints of a 1 km long structure, feasible configurations can be generated using this formulation. The optimization formulation for a structure only defined by PETs or Kreslings can be done by excluding the constraints and parameters not associated with those designs. The Juniper solver [30] was used to solve (31). The configurations found from this optimization for the hierarchical HERDS versus the pure PET or pure Kresling show that HERDS designs find solutions whose objective values are 4–11x better, as seen in Table 4. While the optimization gives kinematically feasible designs, each configuration must be further analyzed with FEA to confirm mission load requirements.

5. STRUCTURE ANALYSIS

Given the design configurations that meet the kinematic requirements of the single launch from the space vehicles, we next assess the additional mission constraints outlined in Section 3. These tests are conducted using Ansys®Academic Research Mechanical, Release 22.2 [28]. The design's hierarchical structure and large part count make a full FEA analysis of the superstructure impractical. Instead, a homogenized model for the substructure beams allows for an effective approximation of superstructure behavior. This is a common approach for approximating global behavior from periodic structures [31]. The superstructure approximation is then evaluated based on the mission-specific force and stress considerations described in Section 3. Finally, we use a Monte Carlo simulation to understand the effects of manufacturing errors on the deployability of the PET mechanism.

Substructure Analysis

Line Body Approximation— Superstructure analysis of this structure would be computationally infeasible due to the large number of parts and the scale of the design. However, approximating the PETs and Kresling as "line bodies" enables much faster system evaluation. In Ansys®, a "line body" represents a one-dimensional entity with a defined cross-section but no surfaces, making it ideal for representing slender structures like beams, rods, and cables. Line bodies can account for bending, axial deformation, and torsion effects. Line bodies can significantly reduce computational resources and time when compared to modeling the full 3D geometry of slender structures. The multi-component PET is approximated as a "line body" with a hollow tube cross-section. This cross-section is designed to have the same total area as the PET cross-section and the same area moment of inertia as the cross-section of the PET that experiences maximum stress. We calculate the homogenized beam cross-section by first running a finite element tension test to compute the effective cross-sectional area (A) based on the constituent material's Young's modulus (E), tension force (F), and strain (ϵ), such that $A_{effective} = \frac{F}{\epsilon E}$. Next, we test the PET bending stiffness by applying a deformation and measuring the resultant force. Approximating the beam as an Euler-Bernoulli beam with aspect ratio > 10, we calculate the effective beam area moment of inertia as $I = \frac{FL^3}{3\delta E}$. We finally solve for a hollow circular cross-section with matching area and moment

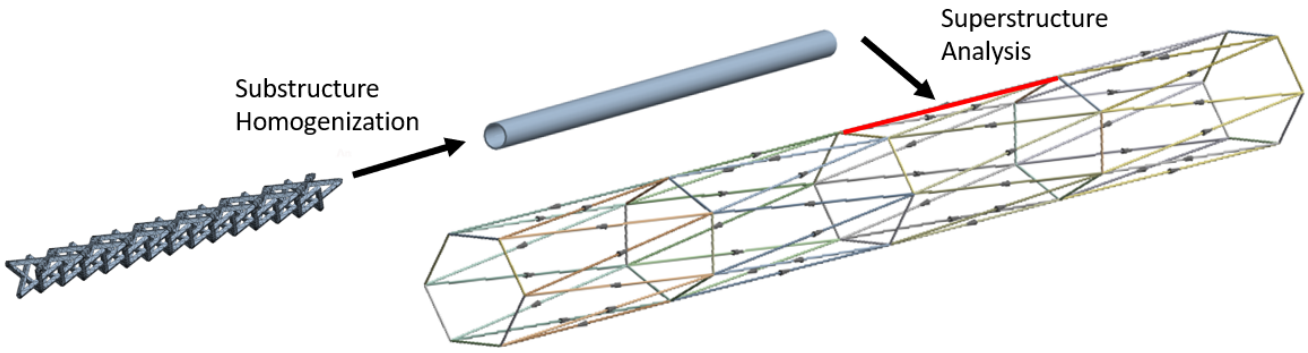

Figure 6. Hierarchical strategy for large scale structural analysis

of inertia with inner and outer diameters:

$$D_i = \frac{\sqrt{8p - \frac{2A^2}{\pi}}}{\sqrt{A}} \tag{33}$$

$$D_o = 2\sqrt{\frac{A}{\pi} - \left(\frac{D_i}{2}\right)^2} \tag{34}$$

While this approximation will not precisely match the original PET, the homogenized version preserves key characteristics and enables functional analysis of the complete structure. To approximate the behavior of the entire 1 km length superstructure, we perform a similar homogenization and apply loads to assess mission-specific requirements.

Superstructure Analysis

The simplified model described in the previous subsection is used to evaluate compressive, tangential, and tensile loading of the complete 1 km structure. As summarized in Table 2, an example target mission may include 300 N thrusters for repositioning and a 20 t payload. In this context, a viable HERDS structure with $9.81 m/s^2$ centripetal acceleration must be able to withstand a minimum tensile force of 0.392400 MN, a minimum compressive force of 300 N, and a minimum torque, $(\tau = 300N * r)$ where r is the radius of the structure, of 200 N-m for Falcon Heavy design, 360 N-m for Starship design and 334 N-m SLS B1 design. From the results displayed in Table 5, we determine a FoS greater than 1.5 for each requirement for all proposed launch fairings. Of the loading conditions, tensile loads result in the lowest FoS. While not included in our model, additional cables may be easily incorporated into the HERDS system to offer additional strength and redundancy. Of the three proposed launch vehicles, the SLS B1 performed the most favorably, with FoS of 4.2 for tension, 17.9 for buckling, and 50.5 for torsion. Such a structure could support much larger habitat designs than existing proposals. Further design optimization leveraging these structural tests in the objective function may provide even greater performance.

Transient Behavior

Jamming—One-degree-of-freedom systems are prone to jamming due to the large number of constraints. The HERDS, hierarchically combining two such systems, necessitated examination in simulations of the sub-structures and superstructure to understand and mitigate this potential failure point. Theoretically, the system's expansion is completely stable; it can be constructed using standard revolute and universal joints. However, manufacturing discrepancies or additional degrees of freedom during transient states may introduce compliance and jamming issues in practice.

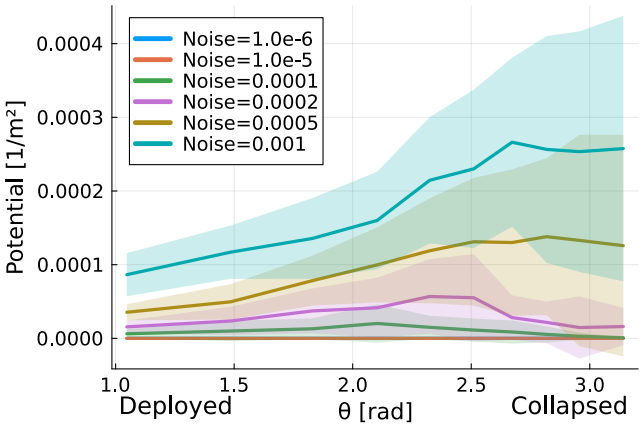

Figure 7. Sensitivity analysis of PET mechanism over 10 poses with varying joint position noise. Fifty design configurations were generated using Monte Carlo sampling. The y-axis is the norm of the joint constraints, which is proportional to potential energy.

In our study, we leverage a Monte Carlo simulation to simulate the influence of tolerance noise on a one-cell PET mechanism. This approach allows us to emulate the inherent uncertainties and variations when joint tolerances are affected by manufacturing processes or other external factors. The tolerance values were varied from 10^{-6} to 10^{-3} meters. For each distinct configuration within this range, we generated 50 individual examples. The goal for each of these examples was to minimize the norm of the joint distances, effectively allowing us to understand the lowest energy configuration for each pose. The resulting data can be seen in Figure 7. This figure's y-axis is proportional to potential energy, while the x-axis is the pop-up phase angle. An interesting observation from the plot is the presence of local minima. These minima indicate regions where the deployment force must overcome an energy barrier to fully deploy and are points where jamming could occur. Lastly, a consistent trend observed across all models is the lower energy in the deployed state. This energy gradient is favorable when minimizing the likelihood of jamming during the superstructure deployment.

Table 5. **Maximum Force analysis of HERDS design and Tether-based Design**

	Max Compressive Load		Max Tensile Load		Maximum Torque	
	[kN]	FOS	[MN]	FOS	[kN-m]	FOS
Falcon Heavy	0.772	2.4	0.618206	1.6	6.581	32.8
Starship	2.367	7.89	0.616321	1.6	5.813	16.14
SLS B1	5.360	17.9	1.664338	4.2	16.868	50.5
Tether	0	0	1.664338	4.2	0	0

Table 6. **Hardware Prototype Parameters**

	Large HERDS	Small HERDS
Thickness	0.006	0.006
PET Cells	13	10
Kresling Cells	2	1
Diameter	0.578	0.298
Initial Height	0.050	0.030
Final Height	2.540	0.488
Expansion Ratio	**50.8**	**16.0**

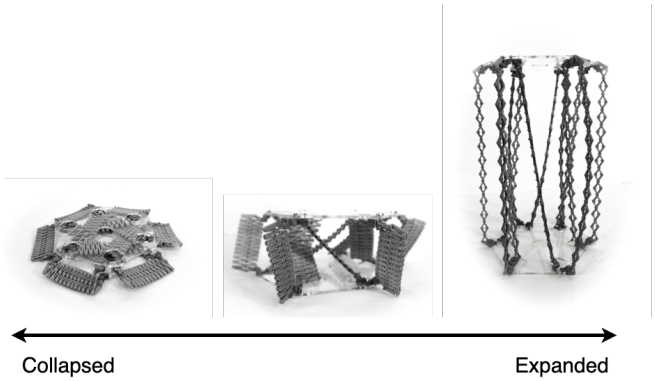

Figure 8. 16x Expansion of small HERDS prototype

Figure 9. 50x expansion of large-scale prototype and PET substructure beams

6. HARDWARE PROTOTYPES

Several physical prototypes were developed to validate our modeling and analysis of the HERDS concept. This section discusses two such prototypes: a small-scale single-cell HERDS (Figure 8) and a large-scale two-cell HERDS (Figure 9). The HERDS were constructed with 3D-printed components, laser-cut acrylic, and metal fasteners. Details, such as joint design and locking strategy, play a prominent role in the system's functionality, and future work must be performed to tune these structures for specific applications. With that in mind, these prototypes demonstrate strong proof of concept and pave the way for future, more refined iterations. The design configuration parameters for each prototype are described in Table 6.

Hardware Testing

For the large prototype, we performed three tests: a deployment test, a compression test, and a three-point bending test. The large prototype was placed in a motion capture system, with markers placed on the middle and top plates to track their position during deployment to measure position and deflection during experiments.

To test effective deployment, we secured a cable to the top plate of the large-scale HERDS, and applied tension to deploy the structure. We did not secure the bottom plate of the HERDS, and the structure extended based solely on the force of gravity. This test primarily validated the feasibility of smooth deployment without jamming or locking. Even with high variability in the more than 2,500 constituent 3D printed parts, we observed no instances of jamming and achieved unified extension. The stowed structure packed to a height of 5 cm and achieved a final length of approximately 254 cm, resulting in just over the targeted 50x expansion ratio.

To test the compressive capabilities of the structure, weights

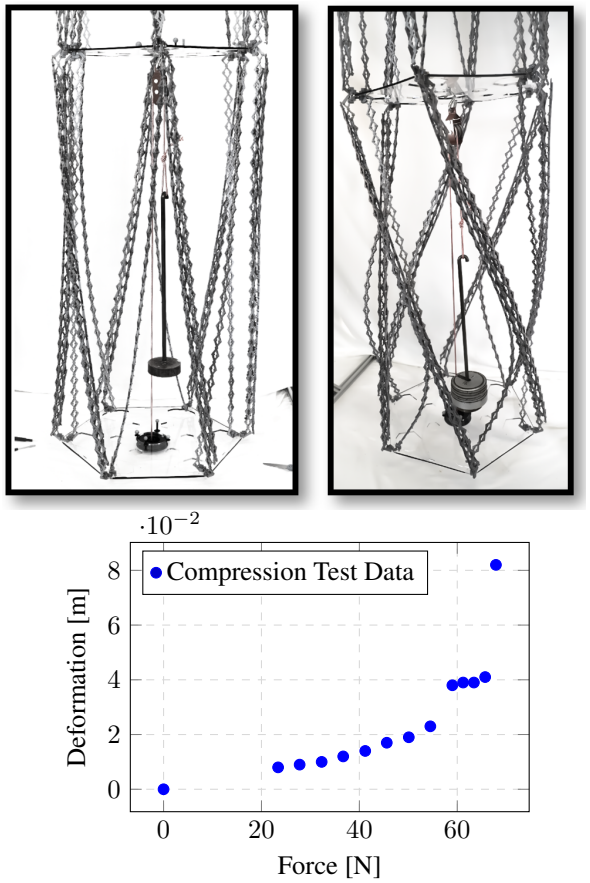

Figure 10. The distance between the bottom two plates upon compressing with discrete weight increments. The measurements were taken until the system reached failure.

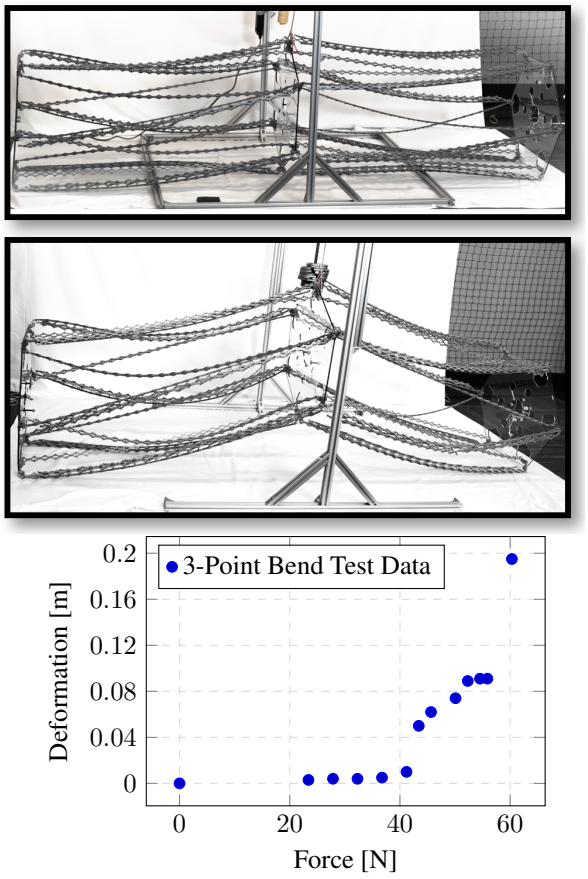

Figure 11. Response of the middle section of a two-cell structure subjected to a 3-point bending test. The measurements were taken until the system reached failure.

were added to a testing setup that can be seen in Figure 10. Weight was incrementally increased until failure, and the deformation between the cell plates was measured using the motion capture system. Results from this test demonstrate that the prototype could support over 60 N force before failure. As a note, the failure was not the breaking of any members but instead plastic deformation of the 3D printed material used to build the structure. While this PLA plastic model is not optimized for structural stiffness, this prototype highlights the significant advantage over a tethered system that could not support any compressive loads.

Finally, a bending test was performed to evaluate the prototype's response to tangential loading conditions. A traditional three-point bending test was inverted due size and space constraints: The test was performed with the two ends of the HERDS beam static on the ground, and the middle of the structure was lifted to apply a force. The results of the displacement of the middle plate are shown in Figure 11. This test showed that the structure primarily deformed at HERDS joint connections, leading to shearing between discrete PET beams, rather than uniform bending. These results motivate additional joint design with improved locking capabilities. Despite these unexpected deformation modes, the model still supported up to 60 N force before failure. Improved locking, tolerances, and base material properties may enhance stiffness and offer enhanced capabilities over tethers.

7. Conclusions

This work provides compelling evidence for the capability of HERDS to meet the demands of single-launch kilometer-scale structures. By leveraging efficient packing to achieve high expansion ratios, HERDS is able to deploy from a single launch and capable of handling compressive loading. We have demonstrated, through simulation and analysis, that HERDS significantly outperforms tether-based approaches under the constraints of the Lunar Gateway mission. Our findings are further solidified by verifying the expansion ratios and loading through hardware prototypes.

Several areas for future work remain: Tolerance coupling and potential jamming risks associated with the complex structure must be better understood. No off-the-shelf software tools currently exist to simulate the system's transient behavior with such a large number of components and joints. Therefore, we are developing a specialized large-scale multi-body simulation code. We also hope to validate HERDS prototypes through additional hardware experiments in a microgravity environment, such as a zero-g flight.

Another major challenge that remains to be studied is maneuvering and station-keeping control, as would be required in a mission like Lunar Gateway. Due to the sheer size of the structure, bending modes will likely need to be actively controlled. The challenge of actuator placement and control of this large structure is still an open area of research.

REFERENCES

[1] T. Lang, J. J. Van Loon, S. Bloomfield, L. Vico, A. Chopard, J. Rittweger, A. Kyparos, D. Blottner, I. Vuori, R. Gerzer, and P. R. Cavanagh, "Towards human exploration of space: the THESEUS review series on muscle and bone research priorities," *npj Microgravity*, vol. 3, no. 1, p. 8, Feb. 2017. [Online]. Available: https://doi.org/10.1038/s41526-017-0013-0

[2] S. Genah, M. Monici, and L. Morbidelli, "The Effect of Space Travel on Bone Metabolism: Considerations on Today's Major Challenges and Advances in Pharmacology," *International Journal of Molecular Sciences*, vol. 22, no. 9, 2021. [Online]. Available: https://www.mdpi.com/1422-0067/22/9/4585

[3] D. R. Roberts, M. H. Albrecht, H. R. Collins, D. Asemani, A. R. Chatterjee, M. V. Spampinato, X. Zhu, M. I. Chimowitz, and M. U. Antonucci, "Effects of Spaceflight on Astronaut Brain Structure as Indicated on MRI," *New England Journal of Medicine*, vol. 377, no. 18, pp. 1746–1753, 2017, _eprint: https://doi.org/10.1056/NEJMoa1705129. [Online]. Available: https://doi.org/10.1056/NEJMoa1705129

[4] J. W. Wolfe and J. D. Rummel, "Long-term effects of microgravity and possible countermeasures," *Advances in Space Research*, vol. 12, no. 1, pp. 281–284, 1992. [Online]. Available: https://www.sciencedirect.com/science/article/pii/027311779290296A

[5] D. Levine and J. Greenleaf, "Immunosuppression during spaceflight deconditioning," *Aviation, space, and environmental medicine*, vol. 69, no. 2, pp. 172–177, Feb. 1998. [Online]. Available: http://europepmc.org/abstract/MED/9491259

[6] J. Rowe, "Artificial Gravity in Mars Orbit for Crew Acclimation," Big Sky, MT, Mar. 2020, nTRS Author Affiliations: Jacobs Engineering Group NTRS Report/Patent Number: M19-7712 NTRS Document ID: 20200002331 NTRS Research Center: Marshall Space Flight Center (MSFC). [Online]. Available: https://ntrs.nasa.gov/citations/20200002331

[7] G. Clément, A. Bukley, and W. Paloski, "History of Artificial Gravity," in *Artificial Gravity*, G. Clément and A. Bukley, Eds. New York, NY: Springer New York, 2007, pp. 59–93. [Online]. Available: https://doi.org/10.1007/0-387-70714-X_3

[8] G. R. Clément, A. P. Bukley, and W. H. Paloski, "Artificial gravity as a countermeasure for mitigating physiological deconditioning during long-duration space missions," *Frontiers in Systems Neuroscience*, vol. 9, 2015. [Online]. Available: https://www.frontiersin.org/articles/10.3389/fnsys.2015.00092

[9] A. Globus and T. Hall, "Space settlement population rotation tolerance," *NSS Space Settlement Journal*, vol. 2, pp. 1–25, 2017.

[10] S. E. T. Corp, "Falcon User Guide," User Guide, Sep. 2021. [Online]. Available: https://www.spacex.com/media/falcon-users-guide-2021-09.pdf

[11] X.-w. Gou, A.-j. Li, H.-c. Tian, C.-q. Wang, and H.-s. Lu, "Overload control of artificial gravity facility using spinning tether system for high eccentricity transfer orbits," *Acta Astronautica*, vol. 147, pp. 383–392, 2018. [Online]. Available: https://www.sciencedirect.com/science/article/pii/S0094576517313681

[12] F. Jensen and S. Pellegrino, "Arm development review of existing technologies," United Kingdom, Tech. Rep. 0309-7447, 2001, cUED/D-STRUCT/TR–198. [Online]. Available: http://inis.iaea.org/search/search.aspx?orig_q=RN:33005654

[13] M. Schenk, A. D. Viquerat, K. A. Seffen, and S. D. Guest, "Review of Inflatable Booms for Deployable Space Structures: Packing and Rigidization," *Journal of Spacecraft and Rockets*, vol. 51, no. 3, pp. 762–778, May 2014, publisher: American Institute of Aeronautics and Astronautics. [Online]. Available: https://doi.org/10.2514/1.A32598

[14] G. Tibert and S. Pellegrino, "Deployable Tensegrity Masts," in *44th AIAA/ASME/ASCE/AHS/ASC Structures, Structural Dynamics, and Materials Conference*, ser. Structures, Structural Dynamics, and Materials and Co-located Conferences. American Institute of Aeronautics and Astronautics, Apr. 2003. [Online]. Available: https://doi.org/10.2514/6.2003-1978

[15] S. Pellegrino, "Deployable Structures in Engineering," in *Deployable Structures*, S. Pellegrino, Ed. Vienna: Springer Vienna, 2001, pp. 1–35. [Online]. Available: https://doi.org/10.1007/978-3-7091-2584-7_1

[16] E. Seedhouse, "Artificial Gravity," in *Pulling G: Human Responses to High and Low Gravity*, E. Seedhouse, Ed. New York, NY: Springer New York, 2013, pp. 169–187. [Online]. Available: https://doi.org/10.1007/978-1-4614-3030-8_9

[17] M. Dobrowolny and N. H. Stone, "A technical overview of TSS-1: The first Tethered-Satellite system mission," *Il Nuovo Cimento C*, vol. 17, no. 1, pp. 1–12, Jan. 1994. [Online]. Available: https://doi.org/10.1007/BF02506678

[18] N. Kong, J. Li, C. Zhang, J. Zhang, H. Li, H. Wang, B. Li, and Y. Wang, "A Study on the Mechanical Characteristics and Self-Preservation Performance of a Deployment Mechanism with a Large Exhibition Ratio during Its Gathering Process," *Materials*, vol. 13, no. 7, 2020.

[19] O. Stohlman and S. Pellegrino, "Shape Accuracy of a Joint-Dominated Deployable Mast," in *51st AIAA/ASME/ASCE/AHS/ASC Structures, Structural Dynamics, and Materials Conference*, ser. Structures, Structural Dynamics, and Materials and Co-located Conferences. American Institute of Aeronautics and Astronautics, Apr. 2010. [Online]. Available: https://doi.org/10.2514/6.2010-2605

[20] N. J. P. Laboratory, "Observatory Unfurls its Unique Mast," News Release, Jun. 2012. [Online]. Available: https://www.nustar.caltech.edu/news/nustar120621

[21] N. A. a. S. Administration, "NASA's Lunar Exploration Program Overview," Program Report, Sep. 2020. [Online]. Available: https://www.nasa.gov/wp-content/uploads/2020/12/artemis_plan-20200921.pdf

[22] S. E. T. Corp, "Starship User Guide," User Guide, Mar. 2020. [Online]. Available: https://www.spacex.com/media/starship_users_guide_v1.pdf

[23] N. A. a. S. Administration, "NASA'S Space Launch System Reference Guide," Tech. Rep. Reference Guide, Aug. 2022. [Online]. Available: https://www.nasa.gov/wp-content/uploads/2022/03/sls_reference_guide_2022_v2_print_0.pdf

[24] R. E. Jones, P. R. Meng, S. J. Schneider,

J. S. Sovey, and R. R. Tacina, "Space Station propulsion system technology," *Acta Astronautica*, vol. 15, no. 9, pp. 673–683, Sep. 1987. [Online]. Available: https://www.sciencedirect.com/science/article/pii/0094576587901391

[25] T. E. S. Agency, "Artemis IV," Tech. Rep., 2022. [Online]. Available: https://www.esa.int/Science_Exploration/Human_and_Robotic_Exploration/Orion/Artemis_IV

[26] J. J. Zipay, C. T. Modlin, and C. E. Larsen, "The Ultimate Factor of Safety for Aircraft and Spacecraft - Its History, Applications and Misconceptions," in *57th AIAA/ASCE/AHS/ASC Structures, Structural Dynamics, and Materials Conference*, ser. AIAA SciTech Forum. American Institute of Aeronautics and Astronautics, Jan. 2016. [Online]. Available: https://doi.org/10.2514/6.2016-1715

[27] H. Segerman and W. Segerman, "Apparatus for branched scissor linkage and associated auxetic mechanisms," U.S. Patent US11 702 327B2, Jul., 2023. [Online]. Available: https://patents.google.com/patent/US11702327B2/en

[28] *ANSYS® Academic Research Mechanical, Release 22 R2*, ANSYS, Inc., 2022, release 22.2.

[29] Z. Zhai, Y. Wang, and H. Jiang, "Origami-inspired, on-demand deployable and collapsible mechanical metamaterials with tunable stiffness," *Proceedings of the National Academy of Sciences*, vol. 115, no. 9, pp. 2032–2037, 2018, _eprint: https://www.pnas.org/doi/pdf/10.1073/pnas.1720171115. [Online]. Available: https://www.pnas.org/doi/abs/10.1073/pnas.1720171115

[30] O. Kröger, C. Coffrin, H. Hijazi, and H. Nagarajan, "Juniper: An Open-Source Nonlinear Branch-and-Bound Solver in Julia," in *Integration of Constraint Programming, Artificial Intelligence, and Operations Research*, W.-J. van Hoeve, Ed. Cham: Springer International Publishing, 2018, pp. 377–386.

[31] B. Hassani and E. Hinton, "A review of homogenization and topology optimization I—homogenization theory for media with periodic structure," *Computers & Structures*, vol. 69, no. 6, pp. 707–717, Dec. 1998. [Online]. Available: https://www.sciencedirect.com/science/article/pii/S004579499800131X

BIOGRAPHY

Mitchell Bennett Fogelson *received his B.S.E and M.S.E from the University of Pennsylvania in Mechanical Engineering in 2017 and Robotics in 2018 respectively. He is currently a Ph.D. candidate in Mechanical Engineering from Carnegie Mellon University. His research includes advanced simulation and optimization methods for mechanical metamaterials and robotic systems.*

Sawyer Thomas *received his B.S. degree in Mechanical Engineering in 2018 from Montana State University. He is currently a Ph.D. Candidate in Mechanical Engineering at the University of Washington. His research focuses on architected transformations in structures and mechanical metamaterials.*

Giusy Falcone *received her B.S. and M.S. degrees in Aerospace Engineering from the University of Pisa in 2014 and 2017, respectively. She then earned her Ph.D. in Aerospace Engineering from the University of Illinois at Urbana-Champaign in 2021. Following her Ph.D., she worked as a Postdoctoral Fellow at Carnegie Mellon University's Robotics Institute within the Robotics Exploration Lab. She is currently an Assistant Professor of Aerospace Engineering at the University of Michigan and serves as the Principal Investigator of the Space-Flight Autonomous Leading Concepts (Space-FALCON) Lab, which specializes in hypersonic and space systems.*

Jeffrey Ian Lipton *received his B.S. in Applied and Engineering Physics in 2010 and Ph.D. in Mechanical and Aerospace Engineering from Cornell University in 2015. He is currently a professor of Mechanical and Industrial Engineering at Northeastern University. His research includes mechanical metamaterials, Robotics, digital fabrication, and deployable structures.*

Zachary Manchester *is an assistant professor in the Robotics Institute at Carnegie Mellon University and founder of the Robotic Exploration Lab. He received a PhD in aerospace engineering in 2015 and a BS in applied physics in 2009, both from Cornell University. His research interests include control and optimization with applications to aerospace and robotic systems.*